Part 1

Guidselines for Book Preparation in MS Word using WSPC Style

Chapter 1

In-silico analytical wear predictions: application to joint prostheses

1.1 Introduction

Wear is a tribological phenomenon occurring to rubbing surfaces, where contact actions and relative sliding cause a loss of volume with surface damage. Therefore, wear is considered one of the main causes of failure of mechanical components, from gears to joint replacements (Fig. 1.1). Wear resistance is generally determined with expensive and time-consuming experimental tests under simplified laboratory conditions. Thus, *in-silico* wear predictions represent an attractive alternative to experimental campaigns, being cheaper and more rapid. Moreover, they can provide indications on wear behavior of rubbing surfaces in realistic working conditions. However, wear simulations are not so widespread today, mainly because the development of models requires some peculiar attentions and it is not easy to check the reliability of results.

This chapter aims to describe *in-silico* wear predictions by means of an analytical approach, in order to provide some practical indications to researchers entering this field. As examples, applications to investigate wear in hip and shoulder prostheses are described. An alternative *in-silico* approach based on the Finite Element method is presented in Chapter X.

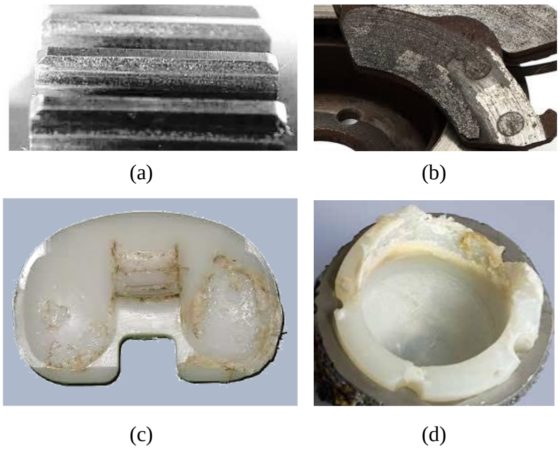

Fig. 1.1. Examples of worn surfaces of mechanical components and biomedical devices: gear (a), disc brake (b), tibial plate of a total knee implant (c), acetabular cup of a hip implants (d).

1.2 Wear modeling: overview

The general procedure for wear estimation is briefly outlined in this section. It consists in several steps:

a) Definition of the relative pose of the two bodies in contact (for the whole simulated time interval) and identification of the nominal contact point. This pose can be determined by solving geometrical (pin-on-disc, cams, etc.) or equilibrium conditions (e.g. hip implants). The latter case is usually more complicated.
b) Mapping of the sliding velocity of the articulating surfaces.
c) Evaluation of the contact actions between the surfaces.
d) Estimation of wear according to the adopted wear law. Both local wear depth h and the total volume loss can be defined as output of this procedure.

Since wear modifies the geometry by removing material, a fifth step can be introduced

e) geometry update (at a proper simulation time).

The procedure is then repeated cyclically until the whole wear process is simulated.

The main difference between the analytical and the FE approach is in the solution of the contact problem, step c). While FE packages can provide the solution for a general contact problem, contact pressure can be analytically estimated only in simple cases. For example, Hertz formulas can be used for non-conformal contacts, while approximated elastic foundation solutions for extended contacts [1, 2].Though the implementation of the geometry update is feasible also in analytical models, it is only rarely performed since the modified geometry could be not suitable for closed form solutions for contact pressure.

The application of the described procedure is illustrated ahead in this chapter focusing on wear predictions for artificial hip and shoulder joints. First, some general observations on the wear law are reported, to highlight the basic concepts of wear formulations.

1.3 Wear law

The fundamental "ingredient" for a wear predictive model is the wear law that is an analytical relationship trying to describe the wear phenomenon, usually under some simplifying assumptions. Indeed, the actual phenomenon is very complex and depends on many factors: micro and macro geometry of the contact coupling, materials, loading conditions, lubrication, temperature etc. Their combination can result in different wear mechanisms: abrasive and/or adhesive wear, fretting, tribocorrosion [3]. Despite the large variety of wear mechanisms, most simulations are based on the Archard's law for abrasive-adhesive wear. It states that, for a translating body, the volume loss V is proportional, via the wear coefficient k, to the product of the normal contact force L_N and the sliding distance s

$$V = k\, L_N\, s \tag{1.1}$$

or, alternatively

$$V = \frac{K}{H}\, L_N\, s \tag{1.2}$$

where H represents the material hardness. The main advantage of the Archard law lies in its simplicity and in the good correlation with experimental evidence.

1.3.1 *Unilateral or bilateral wear*

In Eq.(1.1) the total volume loss V can come from one or both the bodies in contact. When one part is much softer than the other, unilateral wear can be assumed, i.e. only one body gets worn, as in metal on plastic contacts. In case of bilateral wear, both parts get worn and two equations as Eq.(1.1) have to be written to differentiate the wear behavior of the two bodies, i.e.

$$V_1 = k_1 \, L_N \, s \, , \tag{1.3}$$

$$V_2 = k_2 \, L_N \, s \tag{1.4}$$

with $V = V_1 + V_2$ and $k = k_1 + k_2$. However, distinct values of k are only rarely reported in the literature, as well as indications of the separate volumes [4-6]. Most frequently, only one value of k is provided and/or used even when wear is not equally distributed between the bodies [7, 8]. This may be due to the fact that wear, both as phenomenon and as coefficient k, is strongly connected with the coupling more than with single parts. In order to differentiate wear between the two bodies, the present authors have proposed a dimensionless parameter α, named wear partition factor [5], so that

$$k_1 = \alpha \, k \qquad k_2 = (1 - \alpha) k \tag{1.5}$$

and showed its use in simulations in [5, 9].

1.3.2 *Local formulation of the Archard's wear law*

As previously stated, Eq.(1.1) holds only when the relative motion between the rubbing surfaces is a simple translation. In order to deal with a more general case, the Archard's law should be written in a local form to evaluate the wear depth h at a point P moving on a trajectory γ under a pressure p

$$h(P) = k \int_{\gamma} p(P, s)\, ds \tag{1.6}$$

where s is the arc length along γ. Additionally, the relation $s=s(t)$ can be introduced in Eq.(1.6) and h derived to obtain the local wear rate

$$\dot{h}(\mathrm{P}, \mathrm{t}) = k\, p(P, t) |\, \boldsymbol{v}_s(P, t)| \tag{1.7}$$

where $\boldsymbol{v}_s$ is the sliding velocity.

A further generalization of the Archard law can also be found as

$$\dot{h}(\mathrm{P}, \mathrm{t}) = k\, p(P, t)^m \;\; |\, \boldsymbol{v}_s(P, t)|^n \tag{1.8}$$

where pressure and sliding velocity are assumed to have the exponents m and n, respectively.

These local and time-dependent formulations are usually preferred in numerical implementations of wear, in continuous or discrete version.

The total wear volume can be obtained by integrating h over the contact/worn area.

$$V = \int_A h(P)\;dA, \tag{1.9}$$

However, since the geometrical up-date is not implemented, the wear after n loading/wear cycles can be obtained simply by multiplying h and V by n.

1.3.3 *Experimental evaluation of the wear coefficient/law*

The key element in the wear law is the wear coefficient, i.e. k in Eq.(1.1) or $k_{1,2}$ in Eqs.(1.3-4). Usually, it is obtained from standard tests, as pin-on-disc or pin-on-plate wear tests, where a constant normal load L_N is applied to a pin in steady state or cyclic motion with respect to its counterpart. The volume loss V^{exp} is measured by weighting the wear debris or directly the test samples at selected time intervals and/or at the end of the test. Separate measures of samples are needed to estimate $k_{1,2}$. The wear coefficient can be estimated by comparing experimental and numerical (V from Eq.(1.1)) wear volumes obtained under the same conditions, at a given sliding distance s, thus considering $V = V^{exp}$ whence

$$k = V^{\exp} / (L_N\, s) . \qquad (1.10)$$

However, the estimation of a single value for k implies a steady state trend for the phenomenon that in general is not realistic. In most cases, two phases can be identified: a first period of running-in when wear is more rapid and a second phase where wear proceeds more slowly Fig. 1.2. This behavior is described by (at least) two distinct values for k.

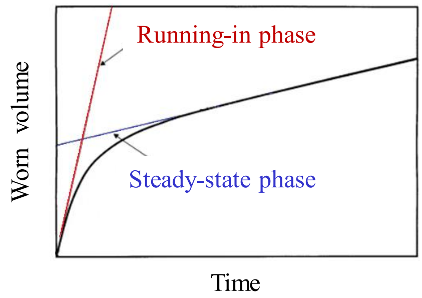

Fig. 1.2. Typical two-phases trend of the wear volume during wear damage process: i) initial running-in phase at high wear rate, and ii) steady state phase at low wear rate.

Another crucial issue is the correlation between results of standard pin-on-disc and pin-on-plate wear tests and the behavior of the components in operative conditions. Since wear depends on many factors, laboratory tests should try to replicate as close as possible the operative conditions of the rubbing parts under examination: geometry, materials, surface finishing, temperature, pressure, lubrication and so on. However, this is almost unfeasible and caution should always be put when using data from tests in practical applications.

1.3.4 *Anisotropic wear: cross-shear phenomenon*

When dealing with wear of plastics, as ultra high molecular weight polyethylene (UHMWPE), the wear coefficient of the Archard's wear law is frequently modified to characterize the anisotropic material behavior. In fact, experimental observations prove that when PE is subjected to multi-directional sliding against a hard counterpart, a principal molecular orientation (PMO) is set in the polymeric chains [10, 11]. In the PMO direction, the wear resistance increases, while in the direction perpendicular to the PMO, named the Cross-Shear direction, wear can occur more easily, Fig. 1.3.

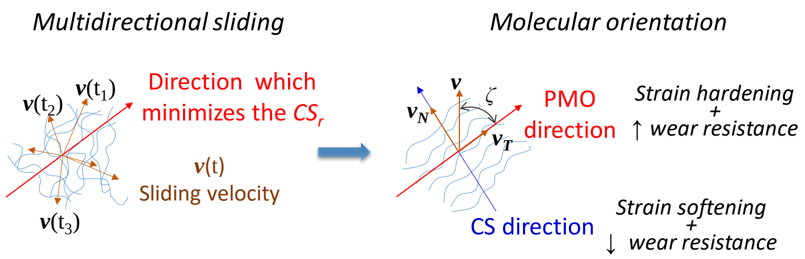

Fig. 1.3. Multi-directional sliding and molecular orientation with identification of the PMO and CS directions. (Adapted and reprinted from [12] with permission from Elsevier).

This anisotropic behavior depends on the point of the surface through a scalar quantity known as the cross-shear ratio (*CS*) defined as the ratio between the frictional work done perpendicularly to the PMO ($W_\perp$) and the total frictional work (W_{tot})

$$CS(P) = \frac{W_\perp}{W_{tot}} = \frac{\int_0^T f\, p(P,t)|\boldsymbol{v}(P,t)|\, \sin^2(\zeta(P,t))\, dt}{\int_0^T f\, p(P,t)|\boldsymbol{v}(P,t)|\, dt} \tag{1.11}$$

where ζ is the angle between the PMO direction and the sliding velocity (Fig. 1.3). The wear coefficient in Eq.(1.1) becomes a function of the point as $k(CS(P))$. The main difficulty in introducing this anisotropy in the model is that the PMO direction is unknown, and it comes from the solution of an optimization problem where PMO is the direction which minimizes $CS(P)$ or, alternatively, $W_\perp$.

Despite the above definition, a kinematic Cross-Shear ratio CS_k is used more frequently

$$CS_k(P) = \frac{\int_0^T |\boldsymbol{v}(P,t)|\,\sin^2\!\big(\zeta(P,t)\big)\,dt}{\int_0^T |\boldsymbol{v}(P,t)|\,dt} \tag{1.12}$$

It comes in case of constant coefficient of friction (CoF) and when the current pressure value is replaced with its average value $\bar{p}$ both in the numerator and denominator so that it can be simplified, (more details in [12]).

The dependence of k on CS_k and on both CS_k and $\bar{p}$ have been proposed by Kang et al. [13, 14] for hip implants and are reported in Table 3.1, with other formulations of k that will be used in the next section. A completely different law will also be considered, proposed by Liu et al. [15], where the nominal contact area A is considered instead of the load

$$V = k_c\,A\,s \tag{1.13}$$

Table 3.1 Wear laws and wear coefficient expressions proposed in the literature for metal-on-UHMWPE couplings, discussed in [12].

Wear law	k/k_c	k/k_c expression (mm^3/(N m))	Ref.
	k cost	$1.066\ 10^{-6}$	[16, 17]
	$k(R_a)$	$(8.68\,R_a + 1.51)\ 10^{-6}$	[18]
$k\,L_N\,s$	$k(CS_k)$	$(0.328\ln(CS_k) + 1.62)\ 10^{-6}$	[13]
	$k(CS_k, \bar{p})$	$exp(-13.1 + 0.19\ln(CS_k) - 0.29\,\bar{p})\ 10^{-6}$	[14]
$k_c\,A\,s$	$k_c(CS_k)$	$\begin{cases} 32\,CS_k + 0.3\,)10^{-9} & CS_k \le 0.04 \\ 1.9\,CS_k + 1.6\,)10^{-9} & 0.04 < CS_k \le 0.5 \end{cases}$	[15]

This synthetic overview of the wear laws does not pretend to provide an exhaustive discussion of the matter, but to present the key issues when developing or choosing a wear law for a predictive model. Other types of laws can be found in the literature, for some specific coupling of materials.

1.4 Prediction of wear in artificial joints

Predictive wear models of artificial joints are particularly important for improving their design, comparing materials, and above all, for simulating realistic working conditions, similar to those observed *in vivo*. The current standards for the experimental evaluation of wear consider fairly simple loading and kinematics conditions (e.g. a kind of simplified gait for hip and knee implants), generally implemented in special simulators. Moreover, experimental campaigns are very expensive and long requiring about 2-5$10^6$ test cycles. *In silico* models can provide indications in shorter times, with a remarkable economic advantage. Above all, they can simulate more closely what happens *in vivo*, during the execution of several different motor tasks. On point of interest in this research is to understand to what extent the regulations are able to evaluate the actual behavior of the prostheses and eventually improve the tests.

At this purpose, predictive wear models were developed based on simple analytical relationships. Indeed, analytical models are rather simple and efficient but do not take into account the modification of the geometry with wear, so they are suitable for 'small wear' and a first estimate. FEM models, presented in Chapter X allow for geometry updates but are quite expensive from a computational point of view [5, 19]. In case of joint replacement, where PE is used in different forms as UHMWPE, XLPE etc., analytical models can be convenient for including the CS effect.

1.4.1 *Hip and shoulder implants*

As example of the analytical approach, the models for two artificial joints are described: those for the widespread hip arthroplasties (HA) and reverse total shoulder arthroplasties (RTSA), re-evaluated in the last decades thank to the modern Grammont design [20] (Fig. 1.4). Though HAs and RTSAs aim at restoring the biomechanics of quite different human synovial joints and, in particular, experience different loading and kinematic conditions, these implants have some common design characteristics and consequently can be treated similarly in wear modelling. Indeed, both of them have a ball-in-socket geometry with the femoral/glenoid head coupled with the acetabular/humeral cup (Fig. 1.4) and are made of the same materials, i.e. plastic/metal for the cup and metal/ceramic both for cup and head [21, 22].

Our investigations were focused on:

(i) Metal-on-plastic (MoP) HAs [12];
(ii) Metal-on-metal (MoM) HAs [9, 23-25];
(iii) Metal-on-plastic RTSAs [26, 27].

The analytical approach combined with a parametric formulation of the model allowed to easily modify model input, from the geometry to the loading/kinematics curves, and the wear laws/coefficients. For this purpose, the software Mathematica® or Mathcad® were employed as they offer powerful tools for symbolic calculus. The developed models were applied for addressing some critical issues highlighted by the literature review and underpinned below:

a) Modeling the cross-shear phenomenon in MoP implants and comparison of the wear laws adopted for UHMWPE [12, 26].
b) Investigations on the effect of the loading and kinematic conditions on wear, by comparing wear predicted for *in-vivo* and *in-vitro* joint simulator BCs [12, 24].
c) Investigations on the effect of implant geometry (size and clearance, related to the dimensional tolerance) on wear [24, 26].
d) Presentation of a novel approach for estimating distinct wear factors for the implant surfaces in case of bilateral wear, i.e. MoM HAs [9].
e) Investigations on the specificity of the wear factor on the tribological scenario: effect of the implant type (MoP HAs vs MoP RTSAs [26]), the implant structure (total vs resurfacing MoM HAs [9]), and the boundary conditions [9] on the wear coefficient.

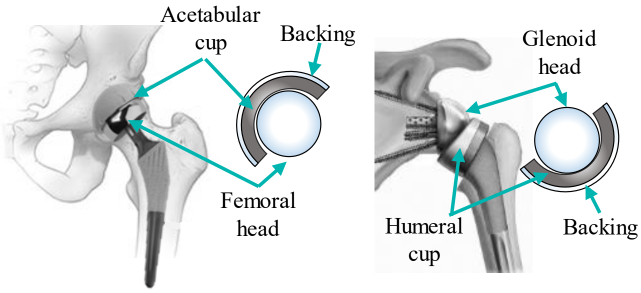

(a) (b)

Fig. 1.4. Hip implant (a) and reverse total shoulder implant (b): images (on the left) and equivalent ball in socket geometry (on the right).

1.4.2 *Models description*

A general analytical wear model of a ball-in-socket couple in case of bilateral wear is presented in this section. The wear models of HAs and RTSAs can be obtained from the general one, making specific simplifications for the implant type.

1.4.2.1 *Model assumptions*

All wear models were based on two hypotheses largely adopted in the literature:

1) The surfaces are considered in dry contact, the lubrication effect being taken into account in the wear coefficient empirically derived.
2) Adhesion and abrasion are considered as the main wear mechanisms, neglecting all the other ones occurring in *in-vivo* (e.g. fatigue, corrosive wear).

Further common basic assumptions are:

3) Geometrical variations due to wear do not affect contact mechanics. That implies that the wear model is suitable for wear prediction during the running-in, i.e. the highest wear rate phase.

4) The contribution of the elastic deformation of cup/head to sliding velocity can be disregarded with respect to the rigid body movements.

Some specific assumptions were called when modeling MoP implants (’)

5’) The wear of the metallic component (head) is negligible with respect to the wear of the plastic side (cup).

6’) The contact is considered frictionless, being f<0.06.

7’) Creep effects are negligible.

or MoM implants (’’):

5’’) The friction coefficient is constant during the running-in phase (f=0.2).

6’’) Contact pressure distribution is not affected by friction, i.e. can be estimated from frictionless contacts.

7’’) The wear coefficient is constant.

It is worth to be stressed that, according to these assumptions, the wear is modelled as unilateral in MoP implants, whilst as bilateral in MoM ones.

1.4.2.2 *Wear laws/model*

In these applications, contact conditions vary in space and time, therefore the local and instantaneous form of the wear law is preferred. More specifically, Eq.(1.8) is used for describing the linear wear rate of a generic point on the cup and head surface, labelled P_c and P_h respectively. Similarly, the cup/head wear coefficients are denoted as k_c/k_h.

1.4.2.3 *Input data*

The model input are listed in the following.

- Geometry: the geometry of ball-in-socket implants is described by the head and cup radii, r_h and r_c, respectively, and by the liner thickness t_c (Fig. 1.5(a)). The position of the cup in the pelvic/humeral bone is specified by the anteversion (α) and the inclination (β) angles (Fig. 1.5(b)). The models were formulated for a left implant using a fixed global frame $C_g=\{O_g; x_g, y_g, z_g\}$ and two mobile frames fixed respectively on the cup, $C_c=\{O_c; x_c, y_c,$

z_c} and on the head, C_h={O_h; x_h, y_h, z_h}, where O_c/O_h are head/cup centers (Fig. 1.5(b)).

- Materials: cup and head material elastic modulus $E_{h,c}$ and Poisson ratio $\nu_{h,c}$. According to the model assumptions, for MoP k_h=0 whilst k_c is defined according to Table 3.1. On the other hand, for MoM HAs, k_h and k_c are considered constant in space and time, i.e. $k_h(P_h,t)=k_h$.
- Loading and kinematic conditions are typically the gait cycle for HA and the mug-to mouth task for RTSAs, considered the most significant for the joints. The BCs consist in the time-history of the contact force (3 components) and the relative orientation between the bodies (expressed as 3 rotations with a specific sequence depending on data source) over a task cycle. Depending on the simulated data, for instance joint simulator or *in-vivo* BCs, the load can be applied to the head or cup, and rotations to a single or both components.

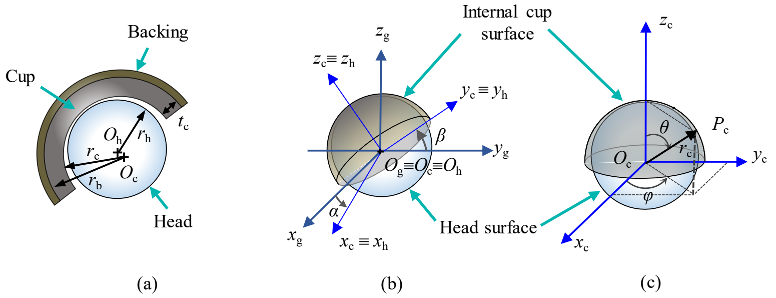

Fig. 1.5. Geometry (a) and coordinate frames (b) of wear models of HA and RTSA. The global frame and the local frames of head and cup are represented in the reference configuration with no loading and null rotations (b). Spherical coordinates used in model implementation (c). (Adapted and reprinted from [12] with permission from Elsevier).

1.4.2.4 *Model implementation*

The model implementation consists in three main steps, described in the following: a) contact analysis; b) kinematic analysis; c) wear assessment. A flow chart of the model implementation is given in Fig. 1.6.

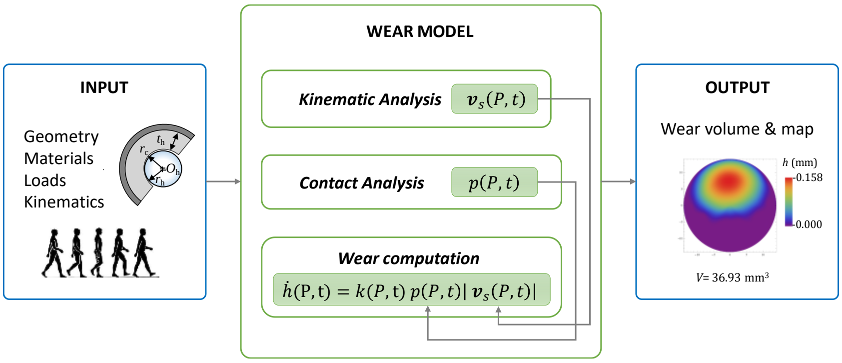

Fig. 1.6. Flow chart of wear model implementation.

a) Contact analysis

The contact analysis consists in two steps:

- Identification of the position of the nominal contact point *K*.
- Estimation of the contact pressure distribution.

For a given set of BCs, the position of *K* is affected by the presence of the friction. In case of frictionless contact, *K* is instantaneously aligned with O_c and O_h, along the load line of action *l* (Fig. 1.7(a)). In presence of friction, *K* is shifted from *l*, of an arc related to the friction angle $\mu = arctan(f)$ with *f* the sliding CoF in the direction opposite to the local sliding velocity, as shown in Fig. 1.7(b, c) [24].

The contact pressure is determined by the normal component L_N of the contact force *L*: in case of frictionless contact $L_N = L$, whilst $L_N = L \cos \mu$ in presence of friction. The pressure distribution over the contact surfaces (red area in Fig. 1.7(d)) was obtained using different approaches, both analytical and numerical, depending on the implant type/materials.

In wear models of a MoP HA [12], a FE contact model was developed for estimating contact pressures under different load levels. By fitting FE results, the pressure distribution was described as

$$p(\psi) = p_{\max}\left(1 - \left(\frac{\sin(\psi)}{\sin(\psi_{\max})}\right)^2\right)^c \tag{1.14}$$

were the maximum contact pressure $p_{\max}$, the semi-angular contact width $\psi_{\max}$ (Fig. 1. 7(d)) and c are functions of the normal load [12].

For MoM HAs, the Hertzian theory was applied though using revised reduced equivalent elastic modulus, estimated considering literature FE results [24]. Differently, Bartel's approximated formulas were assumed to estimate contact pressures in RTSAs wear model [26].

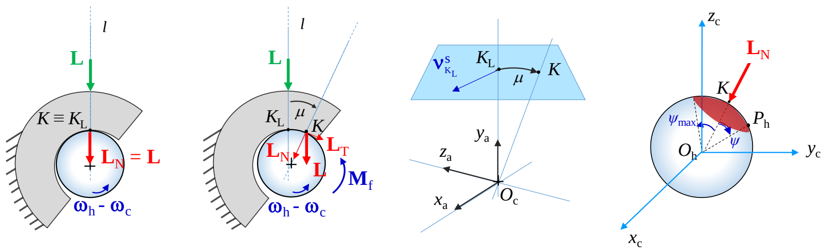

Fig. 1.7. Contact analysis for frictionless (a) and friction (b) contact: external load **L**, nominal contact point *K*. The friction causes the shift of *K* in the opposite direction to the sliding velocity (c) and requires a moment $\mathbf{M}_f$ to overcome frictional resistance. Example of the contact area in red (d). (Reprinted from [24] with permission from ASME).

b) Kinematic analysis

In addition to contact pressure, the other element of the wear law is the sliding velocity. A rigid-body kinematic analysis was therefore implemented, using rotation matrices **R** to define the pose of cup/head.
The position of points P_c/P_h in their own reference frame is time independent and can written for example using spherical coordinates (Fig. 1.5(c)) as

$$[P_i(\theta,\varphi)]_i = [O_iP_i(\theta,\varphi)]_i = r_i\begin{bmatrix} sin\theta\ cos\varphi \\ sin\theta\ sin\varphi \\ cos\theta \end{bmatrix} \quad i\text{=c, h} \tag{1.15}$$

with θ and φ polar and azimuthal angles. In the following, for simplicity, the dependence on such angles will be omitted. Equation (1.15) means that the coordinates of P_i in frame i are equal to the components of the vector O_iP_i in the same frame. Passing in the fixed frame, the coordinates change according to the following

$$\left[O_\mathrm{g}P_i(t)\right]_\mathrm{g} = \left[O_\mathrm{g}O_i(t)\right]_\mathrm{g} + \mathbf{R}_{\mathrm{g}i}(t)[O_iP_i]_i \quad \text{with } i\text{=c, h} \tag{1.16}$$

where $\mathbf{R}_\mathrm{gc}$ and $\mathbf{R}_\mathrm{gh}$ are the rotation matrices that orient respectively the cup and the head frames with respect to the global fix frame. Their general form can be expressed as the scalar products between unit vectors of the reference frames, i.e.

$$\mathbf{R}_\mathrm{gc} = \begin{bmatrix} \boldsymbol{i}_\mathrm{c}\cdot\boldsymbol{i}_\mathrm{g} & \boldsymbol{j}_\mathrm{c}\cdot\boldsymbol{i}_\mathrm{g} & \boldsymbol{k}_\mathrm{c}\cdot\boldsymbol{i}_\mathrm{g} \\ \boldsymbol{i}_\mathrm{c}\cdot\boldsymbol{j}_\mathrm{g} & \boldsymbol{j}_\mathrm{c}\cdot\boldsymbol{j}_\mathrm{g} & \boldsymbol{k}_\mathrm{c}\cdot\boldsymbol{j}_\mathrm{g} \\ \boldsymbol{i}_\mathrm{c}\cdot\boldsymbol{k}_\mathrm{g} & \boldsymbol{j}_\mathrm{c}\cdot\boldsymbol{k}_\mathrm{g} & \boldsymbol{k}_\mathrm{c}\cdot\boldsymbol{k}_\mathrm{g} \end{bmatrix} \tag{1.17}$$

Similarly, for $\mathbf{R}_\mathrm{gh.}$ Such matrices are determined from the kinematic BCs. In a general case, they are time dependent and can be obtained also as a function of the Euler angles. What is typically unknown are the positions of O_c and O_h in the fixed frame. In particular their relative position depends on the contact condition and on the presence of friction as explained above. According to Fig. 1.7, the following vectorial equation can be written

$$O_\mathrm{c}O_\mathrm{h}(t) = -cl\ \boldsymbol{L_N}(t)/|\boldsymbol{L_N}((t)| \tag{1.18}$$

where cl=r_c–r_h is the radial clearance, very small (tens of microns) with respect to both radii. The above equation can be formulated in components in the desired reference frame. In case of frictionless contact $\boldsymbol{L_N}(t)$ is completely known from the BCs ($\boldsymbol{L}$=$\boldsymbol{L}_\mathbf{N}$), while in case of frictional contact $\boldsymbol{L}$=$\boldsymbol{L}_\mathbf{N}$+$\boldsymbol{L}_\mathbf{T}$ and an iterative procedure is required to estimate the sliding velocity and identify the frictional force ($\boldsymbol{L}_\mathbf{T}$) direction.

The absolute velocity of a cup/head point is calculated according to the rigid kinematic law

$$\boldsymbol{v}_{P_i} = \boldsymbol{v}_{O_i} + \boldsymbol{\omega}_i \times O_iP_i \quad i\text{=c, h} \tag{1.19}$$

where $\boldsymbol{\omega}$ is the angular velocity of the element. The relative velocity of a cup point P_c with respect to the head, is given by

$$\boldsymbol{v}_{P_\mathrm{c}}^{\mathrm{r}} = \boldsymbol{v}_{P_\mathrm{c}} - \boldsymbol{v}_{P_\mathrm{h}} = \boldsymbol{v}_{O_\mathrm{c}} + \boldsymbol{\omega}_c \times O_\mathrm{c}P_\mathrm{c} - \left(\boldsymbol{v}_{O_\mathrm{h}} + \boldsymbol{\omega}_\mathrm{h} \times O_\mathrm{h}P_\mathrm{h}\right) \quad (1.20)$$

where P_c is considered overlapped to P_h. Therefore, the relative velocity of a head point with respect to the cup, is

$$\boldsymbol{v}_{P_\mathrm{h}}^{\mathrm{r}} = \boldsymbol{v}_{P_\mathrm{h}} - \boldsymbol{v}_{P_\mathrm{c}} = -\boldsymbol{v}_{P_\mathrm{c}}^{\mathrm{r}} \quad (1.21)$$

Since the clearance is very small, it can be assumed that $O_\mathrm{h}P \approx O_\mathrm{c}P$ so that

$$\boldsymbol{v}_{P_\mathrm{c}}^{\mathrm{r}} \approx \boldsymbol{v}_{O_\mathrm{c}} - \boldsymbol{v}_{O_\mathrm{h}} + (\boldsymbol{\omega}_\mathrm{c} - \boldsymbol{\omega}_\mathrm{h}) \times O_\mathrm{c}P_\mathrm{c} \approx (\boldsymbol{\omega}_\mathrm{c} - \boldsymbol{\omega}_\mathrm{h}) \times O_\mathrm{c}P_\mathrm{c} \quad (1.22)$$

where relative velocity of O_h with respect to O_c is considered neglegible. It has been checked that for HAs, the above simplification introduces an error <0.5%.

Finally, the sliding velocity $\boldsymbol{v}_P^{\mathrm{s}}$ can be obtained considering the tangential component of the relative velocity, i.e.

$$\boldsymbol{v}_{P_i}^{\mathrm{s}} = \boldsymbol{v}_{P_i}^{\mathrm{r}} - \frac{\left(v_{P_i}^{\mathrm{r}} \cdot O_iP_i\right)}{r_i^2} O_iP_i \quad i=\mathrm{c, h} \quad (1.23)$$

The simplified version of the relative velocity in Eq.(1.22) can be used to rapidly estimate the sliding velocity.

The sliding velocity is necessary also for determining $\boldsymbol{L}_\mathbf{N}$ in frictional conditions, being

$$\boldsymbol{L}_\mathbf{N} = \boldsymbol{L} - \boldsymbol{L}_\mathbf{T} = \boldsymbol{L} - \sin(\mu)\,|\boldsymbol{L}|\,\boldsymbol{s}_\mathbf{v}, \quad \text{where} \quad \boldsymbol{s}_\mathbf{v} = \boldsymbol{v}_{P_\mathrm{h}}^{\mathrm{s}} \Big/ \left|\boldsymbol{v}_{P_\mathrm{h}}^{\mathrm{s}}\right| \quad (1.24)$$

Usually, depending on the BCs, the head or the cup center is considered fixed and the above equation can be further simplified.

c) Wear assessments

The wear is evaluated both as wear depth and wear volume on both bodies. The wear depth h at a cup/head surface point, in a loading cycle of period T can be obtained adapting Eq.(1.6) as

$$h(P_\mathrm{c}) = \int_0^T \dot{h}(P_\mathrm{c}, t)\ dt \ , \quad h(P_\mathrm{h}) = \int_0^T \dot{h}(P_\mathrm{h}, t)\ dt \tag{1.25}$$

and similarly the wear volumes from Eq.(1.9)

$$V_\mathrm{c} = \int_{A_\mathrm{c}} h(P_\mathrm{c})\ dA \ , \quad V_\mathrm{h} = \int_{A_\mathrm{h}} h(P_\mathrm{h})\ dA \tag{1.26}$$

It should be reminded that, according to Eq.s (1.3-4)

$$V_\mathrm{c} : V_\mathrm{h} = k_\mathrm{c} : k_\mathrm{h} \tag{1.27}$$

In these models, it is also assumed that no significant modification of the contact surfaces occurs (no geometrical up-date), so that wear after *n* loading cycles can be obtained simply by multiplying *h* and *V* by *n*.

1.4.3 *Wear simulations of MoP HA*

1.4.3.1 *Effect of wear laws*

Wear investigations presented in [12] were focused on the comparison of the wear laws for UHMWPE discussed in §1.3.4 (Table 3.1). In particular, the aim was to investigate the role of the cross-shear effect on UHMWPE wear.

Wear maps predicted for a 14 mm implant under *in-vivo* BCs are compared in Fig. 1.8. All wear laws predict high linear wear in the regions that experience the maximum contact pressure. Qualitatively, the wear maps predicted using the Archard wear law are very similar independently from *k* expressions, whilst a much different wear map is obtained for the new wear law (Eq.1.13), which estimates a wider region affected by the maximum wear depth (top of Fig. 1.8). On the other hand, quantitatively, wear indicators are significantly affected by the wear laws/coefficients with the lowest h_{max} and *V* values observed for the new wear law (bottom of Fig. 1.8(a-d)). The results demonstrate the relevance of CS modeling and the necessity to validate wear laws/coefficients by comparing numerical and experimental wear predictions obtained for the same implant, under the same conditions.

1.4.3.2 *Effect of BCs*

The operating conditions of an implant, i.e. loading and kinematics conditions, can greatly influence its wear. This aspect has been investigated in [12]. In particular, a key point was to understand whether the simplified gait conditions assumed in joint simulators for wear testing are suitable to predict the *in-vivo* scenario. Results demonstrate that the implant wear is more sensitive to the kinematic conditions than to the loading ones, and that the wear rates under *in-vitro* BCs underestimate the *in-vivo* ones, with percentage variations of $h_{\max}$ and V up to 44% and 28%, depending on the wear laws (Fig. 1.9(b)). As an example, Fig. 1.9(a, b) shows the wear maps obtained for two wear laws in *in-vitro* BCs that result qualitatively and quantitatively different from the correspondent ones obtained under *in-vivo* BCs and portrayed in Fig. 1.8(d, e).
Accordingly, results strongly encourage the simulation of more physiological-like BCs in joint simulator wear tests.

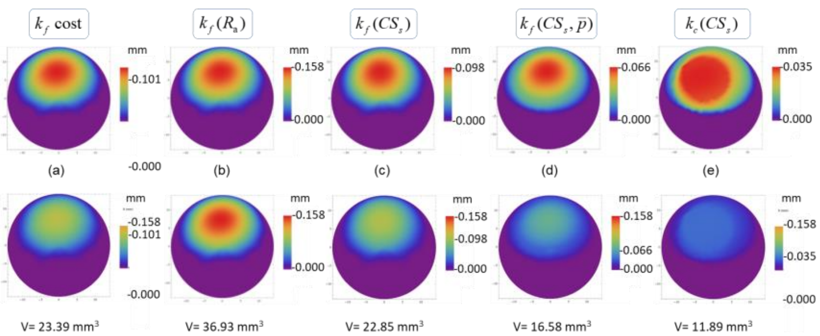

Fig. 1.8. Linear and volumetric wear at 1 Mc of the plastic cup of a 14 mm MoP HA (in the $x_c y_c$ plane) under *in-vivo* gait conditions, predicted using different wear laws. Maps are drawn both on different scales, within its own minimum and maximum values (top) and on the same scale (bottom). (Reprinted from [12] with permission from Elsevier).

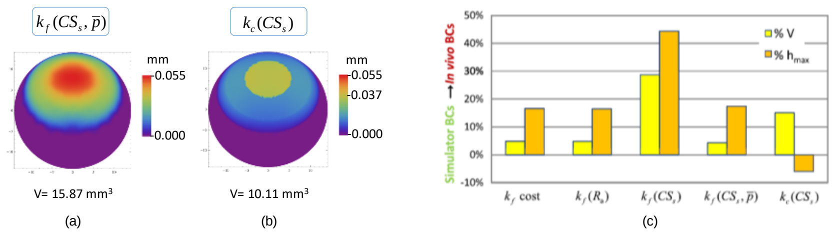

Fig. 1.9. Wear maps and volumetric wear at 1 Mc of the plastic cup of a 14 mm MoP HA (in the $x_c y_c$ plane) under joint simulator conditions, predicted using different wear laws (a, b). Percentage variation of h_{max} and V between *in-vitro* and *in-vivo* BCs (c). (Reprinted from [12] with permission from Elsevier).

1.4.4 *Wear simulations of MoM HA*

1.4.4.1 *Effect of friction*

Wear models of MoM HAs have two main peculiarities with respect to the previous ones: bilateral wear and frictional contact.
The presence of friction, as already exposed in §1.4.2.3, affects the normal load component and its point of application. In particular, it results in wider trajectories of the nominal contact point K, both on head and cup surfaces [23, 24]. This is well depicted in Fig. 1.10 (a, d) that compare the frictionless and friction predictions for a 14 mm HAs under *in-vivo* gait conditions. Accordingly, the friction causes a wider worn area, with lower wear depths, and also a lower volumetric wear (Fig. 1.10(e, f) vs (b, c)).

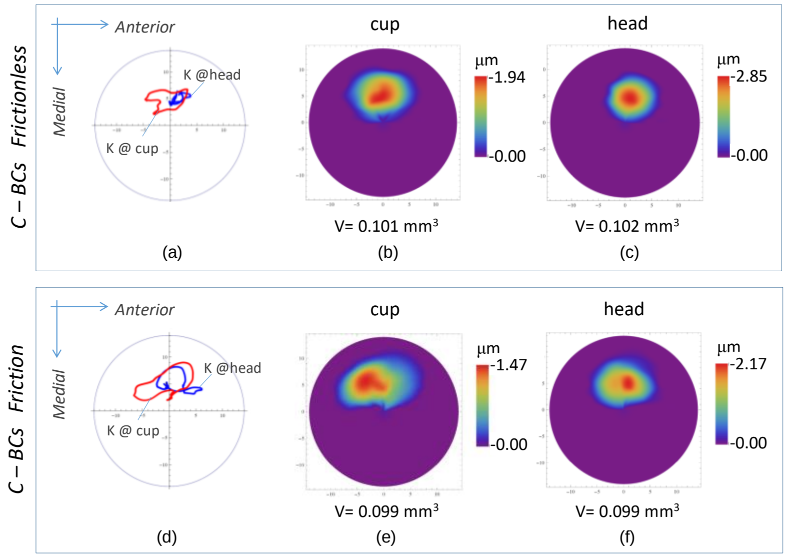

Fig. 1.10. Linear and volumetric wear at 1 Mc for a 14 mm MoM HA, under in-vivo BCs: frictionless contact (top) vs frictional contact (bottom). (a) Trajectories of the nominal contact point K on cup and head; wear map on the cup (b, e) and on the head (c, f). (Reprinted from [24] with permission from ASME).

1.4.4.2 *Estimation of distinct wear coefficients for head and cup*

Wear models can also be useful for estimating the coefficient k from wear tests directly performed on the components, for example using hip simulators. In this case, Eq.(1.1) cannot be simply inverted as in Eq.(1.10), but the general form for the volume loss in Eq.(1.26) has to be used. Assuming a constant wear coefficient, the linear wear depth becomes

$$h(P_i) = k_i \int_\gamma p(P_i, s)\, ds = k_i\ \tilde{h}(P_i) \qquad i = \mathrm{c}, \mathrm{h} \tag{1.28}$$

and the wear volume

$$V_i = \int_{A_i} h(P_i)\ dA = k_i \int_{A_i} \tilde{h}(P_i)\ dA \tag{1.29}$$

This expression compared to the experimentally measured volume loss, V^{exp}, provides the formula for k estimation

$$k_i = \frac{V_i^{\mathrm{exp}}}{\int_{A_i} \tilde{h}(P_i)\, dA} \qquad i = \mathrm{c}, \mathrm{h} \tag{1.30}$$

This procedure was applied in [9, 25] to estimate the wear coefficients for the head and cup, employing data of distinct wear volumes for the two components available in few literature studies. and used to estimate k_h and k_c, in place of the traditional average of the two frequently used. Results for the case taken from [28] are shown in Fig. 1.11: k_h is about two-fold k_c and causes the highest linear wear in the head. This is in agreement with the experimental data (V_h>V_c) and can be explained considering the simulated loading conditions: indeed, being the load fixed on the head, the head worn more than the cup. Results demonstrate the relevance to use distinct wear factor for the coupling samples in order to obtain reliable wear predictions.

The novel approach was also applied to evaluate the influence of the implant geometry, i.e. size and clearance, on wear coefficient, both for total and resurfacing implants [9]. By comparing implants subjected to the same BCs, it resulted that the higher the head radius and the lower the clearance, the lower the wear coefficient. Indeed, in both cases the bearing is more conformal and the lubrication is promoted reducing the wear.

Results confirmed that the high specificity of the wear coefficient values to the simulated tribological scenario including, in addition to implant materials, implant size and dimensional tolerance, loading and kinematic conditions.

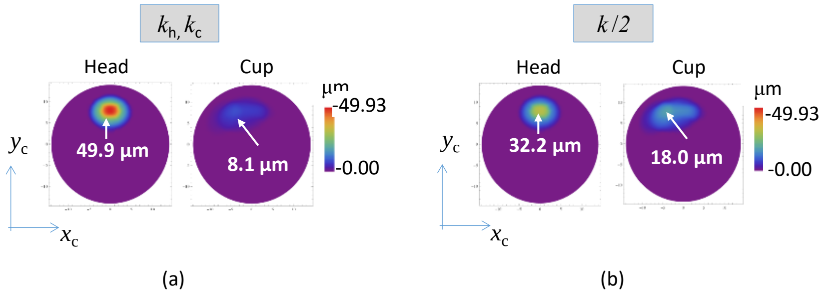

Fig. 1.11. Linear and volumetric wear at 1 Mc for a 14 mm MoM HA, under *in-vitro* BCs, using specific cup and head wear coefficients (a), or the traditional $k/2$ for both the elements. (Adapted and reprinted from [9] with permission from Elsevier).

1.4.5 *Wear simulations of MoP RTSA*

1.4.5.1 *Estimation of specific wear coefficients for RTSA*

The first objective in wear investigations on RTSAs was to evaluate specific k values for this implant type. Indeed, wear models of RTSAs available in the literature adopt the same values of the wear coefficient for MoP HAs. Given the high specificity of k on the tested conditions, that can cause high error in wear predictions. In [26], experimental wear data on a 42 mm RTSA were used to estimate k using both the Archard and the UHMWPE (Eq.1.13) wear laws. Results demonstrated that the wear coefficients differ significantly for MoP RTSAs and HAs, despite the same coupled materials, and are higher (up to two-fold) for the RTSAs. The computed k were then used to predict wear maps and investigate how they are affected by the wear laws/coefficients. Results are shown in Fig. 1.12 and are in well agreement with those ones of MoP HA of Fig. 1.8: the wear maps predicted by the two wear laws differ significantly, although associated to the same wear volume. The new wear law predicts lower linear wear rates compared to the Archard one, with the maximum wear depth located at the edge of the worn area and not at the cup dome.

Consequently, the necessity of a model validation through both wear volume and wear maps is confirmed.

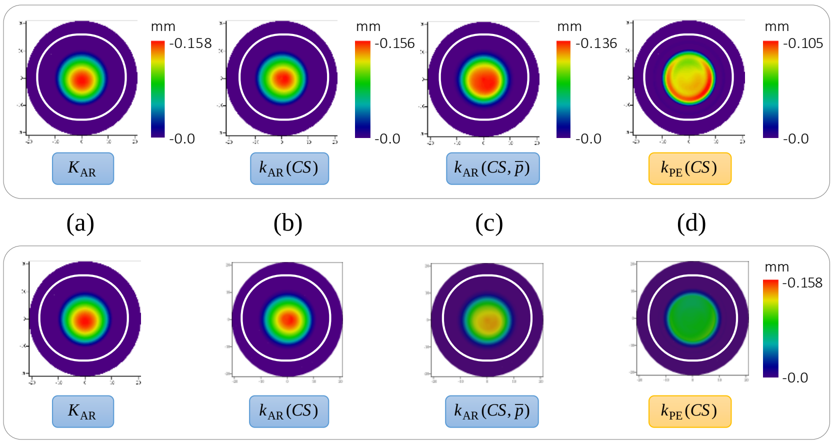

Fig. 1.12. Linear wear at 2 Mc of the plastic cup of a 42 mm MoP RTSA (in the $x_c y_c$ plane) for a mug-to mouth task, predicted using different wear laws (V=26.6 mm^3). Maps are drawn both on different scales, within its own minimum and maximum values (top) and on the same scale (bottom). (Reprinted from [26] with permission from Elsevier).

1.4.5.2 *Effect of size and dimensional tolerance on wear*

The effect of the implant geometry on wear was investigated also for RTSA [27], using the implant-specific k evaluated in [26]. The focus was not only on the implant size (i.e. d_h), but also on the dimensional tolerance. The latter plays a fundamental role in the implant tribological performance since it is directly related to the clearance, and thus to the contact conditions and the lubrication regime. However, rather surprisingly, it is not indicated in standards, nor discussed in the literature. A set of 10 different geometries was analysed, considering nominal diameters in the range 36-42 mm, available on the market, and a cup dimensional tolerance of +0.2-0.0 mm [27]. The results of the wear sensitivity analysis to cl and d_h are summarized respectively in Fig. 1.13 and Fig. 1.14, for different wear laws. They demonstrated that wear indicators are affected by both implant size and dimensional tolerance, although they are more sensitive to the latter. As the implant conformity decreases – for smaller d_h and/or higher *cl* – the volumetric wear increases, according to both wear laws. On the other hand, the linear wear is only slightly affected by the implant size, whilst is highly influenced by the *cl*. However, different trends are predicted by the two wear laws: according to the Archard wear law, the higher the *cl*, the higher the wear depths, in opposite to the UHMWPE law. These investigations remark the need to validate both wear laws and wear models and the high sensitivity of *k* to the implant geometry, as well as the necessity to specify stringent limits on the dimensional tolerance in standards.

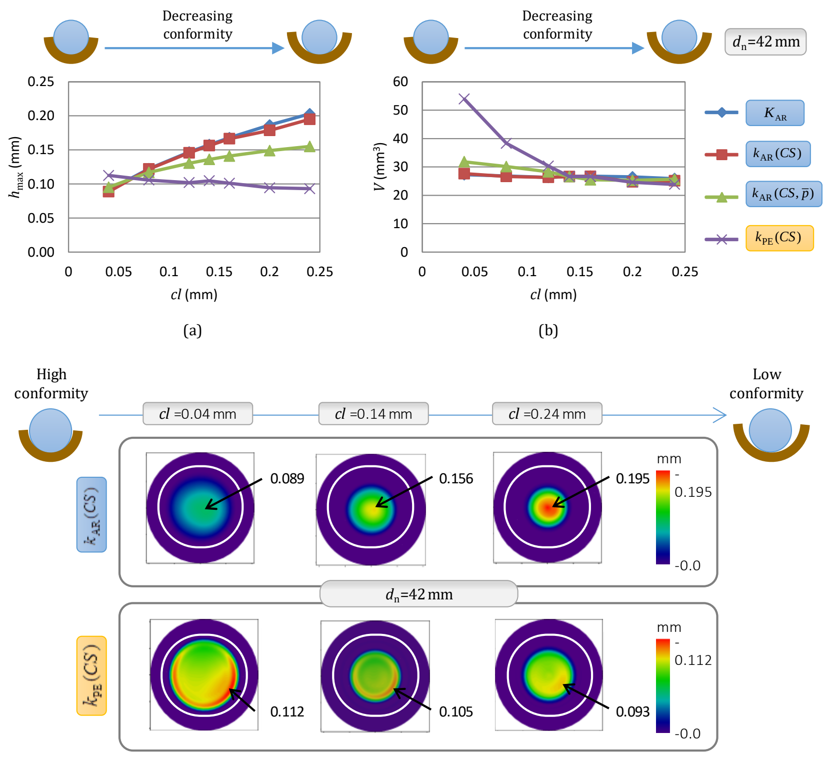

(c)

Fig. 1.13. Effect of the dimensional tolerance (i.e. *cl*) *cl* on linear wear (a, c) and volumetric wear (b), for a 42 mm RTSA. Comparison of wear predictions for different wear laws and wear coefficients. (Reprinted from [27] with permission from Elsevier).

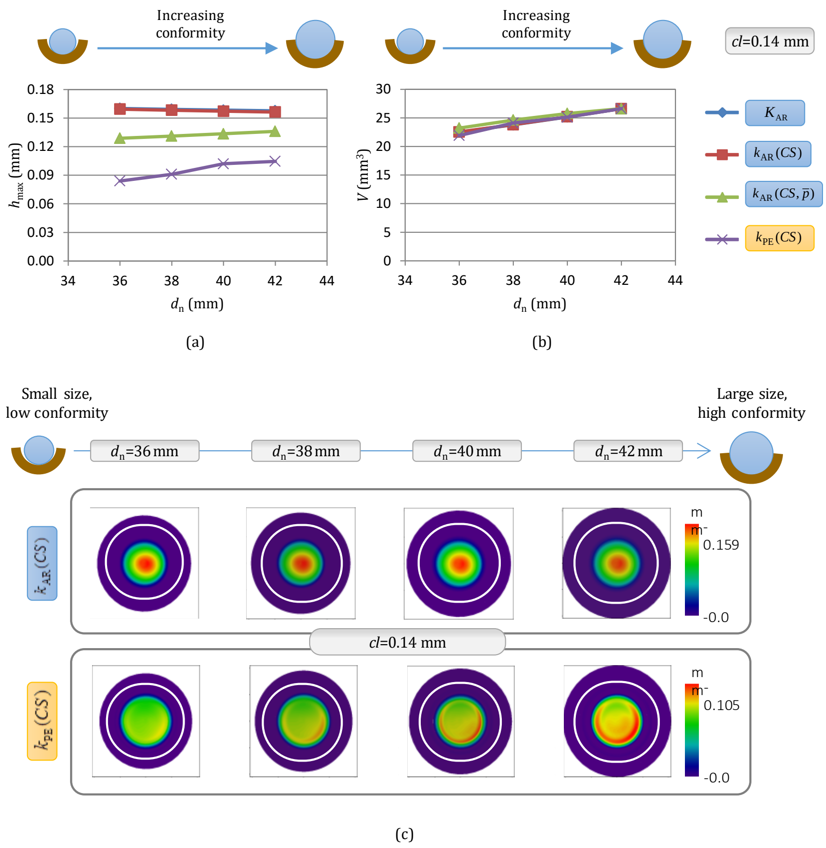

Fig. 1.14. Effect of the size (i.e. r_h) on linear wear (a, c) and volumetric wear (b), for a 42 mm RTSA (*cl*=0.14 for all implants). Comparison of wear predictions for different wear laws and wear coefficients. (Reprinted from [27] with permission from Elsevier).

1.4.6 *Wear law/model validity*

The wear law and wear model validity are strictly related and should be assessed by comparing numerical predictions to experimental results obtained simulating the same tribological scenario (e.g. same test samples, operating conditions, etc.). Attention should be paid to this key point. Since the wear coefficient (considered constant) is obtained by comparing V and V^{exp} (Eq.s(1.10,30)), the wear model validation needs the comparison of another wear indicator, i.e. the linear wear over the worn surface, generally name wear map. However, this approach is rarely considered and often a “dependent” model validation is declared based only on wear volumes. One of the reasons, is that in some cases wear maps reconstruction can be very difficult and costly as it happened for very conformal contacts such as in hip and shoulder implants, for whom wear maps are rarely collected rarely collected. Obviously, the wear law/model validation is even more complicated in case of not constant k (Table 3.1). Recently, the literature has raised this issue and some attempts of wear maps reconstruction have been proposed [29].

1.5 Conclusions

Wear predictive models represent an attractive alternative to expensive and long experimental tests. In the recent years, FE simulations have been proposed to investigate wear in mechanical components. However, the analytical approach described in this Chapter is still a good option for more rapid indications. The described examples on hip and shoulder implants show the simplicity of the implementation also in presence of complex wear laws, as those needed by UHMWPE surfaces.

The main limit of analytical models is represented by the estimation of contact actions, based on literature formulas (e.g. Hertz, Winkler etc.). Typically, the initial unworn geometry is maintained for the entire simulation, assuming the geometry modifications due to wear can be neglected. This can be true for an initial period, usually correspondent to the running-in. However, volume loss estimated by analytical models are in good agreement also with experimental test results.

Further aspects are discussed in the Chapter on FE approach.

1.6 References

[1] K.L. Johnson, Contact mechanics, Cambridge University Press, Cambridge Cambridgeshire ; New York, 1985.
[2] H.R. Hertz, On Contact Between Elastic Bodies, Leipzig, Germany, 1882.
[3] I. Hutchings, P. Shipway, Tribology, Butterworth-Heinemann, 2017.
[4] J. Lengiewicz, S. Stupkiewicz, Efficient model of evolution of wear in quasi-steady-state sliding contacts, Wear, 303 (2013) 611-621.
[5] L. Mattei, F. Di Puccio, Influence of the wear partition factor on wear evolution modelling of sliding surfaces, Int J Mech Sci, 99 (2015) 72-88.
[6] I.R. McColl, J. Ding, S.B. Leen, Finite element simulation and experimental validation of fretting wear, Wear, 256 (2004) 1114-1127.
[7] J. Andersson, A. Almqvist, R. Larsson, Numerical simulation of a wear experiment, Wear, 271 (2011) 2947-2952.
[8] N.H. Kim, D.K. Won, D. Burris, B. Holtkamp, G.R. Gessel, P. Swanson, W.G. Sawyer, Finite element analysis and experiments of metal/metal wear in oscillatory contacts, Wear, 258 (2005) 1787-1793.
[9] F. Di Puccio, L. Mattei, A novel approach to the estimation and application of the wear coefficient of metal-on-metal hip implants, Tribol Int, 83 (2015) 69-76.
[10] A. Wang, D.C. Sun, S.S. Yau, B. Edwards, M. Sokol, A. Essner, V.K. Polineni, C. Stark, J.H. Dumbleton, Orientation softening in the deformation and wear of ultra-high molecular weight polyethylene, Wear, 203-204 (1997) 230-241.
[11] M. Turell, A. Wang, A. Bellare, Quantification of the effect of cross-path motion on the wear rate of ultra-high molecular weight polyethylene, Wear, 255 (2003) 1034-1039.
[12] L. Mattei, F. Di Puccio, E. Ciulli, A comparative study on wear laws for soft-on-hard hip implants using a mathematical wear model, Tribol Int, 63 (2013) 66-77.
[13] L. Kang, A.L. Galvin, T.D. Brown, J. Fisher, Z.M. Jin, Wear simulation of ultra-high molecular weight polyethylene hip implants by incorporating the effects of cross-shear and contact pressure, Proceedings of the Institution of Mechanical Engineers, Part H (Journal of Engineering in Medicine), 222 (2008) 1049-1064.
[14] L. Kang, A.L. Galvin, J. Fisher, Z. Jin, Enhanced computational prediction of polyethylene wear in hip joints by incorporating cross-shear and contact pressure in additional to load and sliding distance: Effect of head diameter, J Biomech, 42 (2009) 912-918.

[15] F. Liu, A. Galvin, Z. Jin, J. Fisher, A new formulation for the prediction of polyethylene wear in artificial hip joints, Proceedings of the Institution of Mechanical Engineers, Part H: Journal of Engineering in Medicine, 225 (2011) 16-24.
[16] T. Maxian, T. Brown, D. Pedersen, J. Callaghan, 3-dimensional sliding-contact computational simulation of total hip wear, Clin Orthop Relat Res, 333 (1996) 41-50.
[17] T.A. Maxian, T.D. Brown, D.R. Pedersen, J.J. Callaghan, A sliding-distance-coupled finite element formulation for polyethylene wear in total hip arthroplasty, J Biomech, 29 (1996) 687-692.
[18] M.T. Raimondi, C. Santambrogio, R. Pietrabissa, F. Raffelini, L. Molfetta, Improved mathematical model of the wear of the cup articular surface in hip joint prostheses and comparison with retrieved components, Proc Inst Mech Eng H J Eng Med, 215 (2001) 377-391.
[19] C. Curreli, F. Di Puccio, L. Mattei, Application of the finite element submodeling technique in a single point contact and wear problem, International Journal for Numerical Methods in Engineering, 116 (2018) 708-722.
[20] P. Boileau, D.J. Watkinson, A.M. Hatzidakis, F. Balg, Grammont reverse prosthesis: Design, rationale, and biomechanics, J Shoulder Elbow Surg, 14 (2005) S147-S161.
[21] F. Di Puccio, L. Mattei, Biotribology of artificial hip joints, World J Orthop, 6 (2015) 77-94.
[22] L. Mattei, F. Di Puccio, B. Piccigallo, E. Ciulli, Lubrication and wear modelling of artificial hip joints: a review, Tribol Int, 44 (2011) 532–549.
[23] L. Mattei, F. Di Puccio, E. Ciulli, Wear simulation of metal on metal hip replacements: An analytical approach, in: 11th ASME Biennial Conference on Engineering Systems Design and Analysis, ESDA 2012, 2012, pp. 555-564.
[24] L. Mattei, F. Di Puccio, Wear simulation of metal-on-metal hip replacements with frictional contact, J Tribol, 135 (2013) 1-11.
[25] L. Mattei, F. Di Puccio, E. Ciulli, Estimation of wear factors of metal-on-metal hip implants from simulator tests, in: 5th World Tribology Congress, WTC 2013, Torino, IT, 2013, pp. 413-416.
[26] L. Mattei, F. Di Puccio, T.J. Joyce, E. Ciulli, Numerical and experimental investigations for the evaluation of the wear coefficient of reverse total shoulder prostheses, J Mech Behav Biomed Mater, 55 (2016) 53-66.
[27] L. Mattei, F. Di Puccio, T.J. Joyce, E. Ciulli, Effect of size and dimensional tolerance of reverse total shoulder arthroplasty on wear: An in-silico study, J Mech Behav Biomed Mater, 61 (2016) 455-463.

[28] S. Williams, D. Jalali-Vahid, C. Brockett, Z. Jin, M.H. Stone, E. Ingham, J. Fisher, Effect of swing phase load on metal-on-metal hip lubrication, friction and wear, J Biomech, 39 (2006) 2274-2281.
[29] L. Mattei, F. Di Puccio, E. Ciulli, A. Pauschitz, Experimental investigation on wear map evolution of ceramic-on-UHMWPE hip prosthesis, Tribol Int, 143 (2020) 106068.